PERGAMON

International Journal of Heat and Mass Transfer 45 (2002) 1425–1444

International Journal of HEAT and MASS TRANSFER

www.elsevier.com/locate/ijhmt

Transient natural convection in a cylindrical enclosure at high Rayleigh numbers

E. Papanicolaou *, V. Belessiotis

Solar and Other Energy Systems Laboratory, "Demokritos" National Center for Scientific Research, Aghia Paraskevi, Attiki 15310, Greece

Received 19 February 2001; received in revised form 16 July 2001

Abstract

The transient state of natural convection in a vertical cylindrical enclosure is studied numerically for water at high Rayleigh numbers, extending into values characteristic of the turbulent flow regime. Several two-equation turbulence models are used for this purpose. Heating is provided along the cylindrical surface at a constant heat flux, with the horizontal bounding surfaces being adiabatic and the development of stratification is studied. Such a configuration is very relevant to thermal storage tanks or solar thermal system vessels and the study aims at providing insight into the behavior of the system at the boundary between laminar and turbulent flow so that the appropriate numerical treatment may be adopted in future studies. The main aspect ratio considered is $L/D = 1$ and the Rayleigh number (based on the length L) varies in the range $10^{10} \geqslant Ra \geqslant 10^{13}$ for laminar flow and $5 \times 10^{13} \geqslant Ra \geqslant 10^{15}$ for turbulent flow, values for which previous data in the literature are all but non-existent. The attainment of a quasi-steady state is achieved after the fluid undergoes an oscillating pattern where secondary flows alternately appear and vanish. These patterns affect the development of stratification in the vessel. Low-Reynolds k–ϵ models predict eventually a relaminarization at large times, but models employing the high-Re form of the k–ϵ model obtain sustained or very slowly decaying turbulence instead. Comparisons are made with experimental results where applicable. © 2002 Published by Elsevier Science Ltd.

1. Introduction

Thermal energy storage, whether in the form of sensible or latent heat, is significantly affected by natural convective flow and associated heat transfer. During the charging or discharging of a liquid storage tank, but also in its still phase where there is heat exchange with the surroundings, natural convection significantly affects the efficiency of storage. It also plays a very important role in the performance of vessels which are part of thermosyphon-type solar water heating systems [1,2]. In order to properly analyze the relative phenomena, the basic aspects of natural convective flows and transport need to be well understood and have, therefore, been the subject of investigation by many researchers in the past, both in rectangular and, to a lesser extent, in cylindrical geometries. As far as rectangular enclosures are concerned, the basic problem of natural convection has been quite extensively studied in both the laminar and the turbulent flow regimes, the physics has been well analyzed and numerical simulations have produced well documented, benchmarked results [3,4]. Cylindrical geometries on the other hand have received more limited attention as far as the fundamental problem is concerned. Among the earliest representative studies in vertical cylinders were those presented by Evans et al. [5], Hess and Miller [6,7] who carried out both analytical and experimental works and Daney [8] who carried out experimental work. Numerical studies on vertical cylinders have been presented by Shyu and Hsieh [9], Hyun [10], Lin and Akins [11,12], Sun and Oosthuizen [13], Lemembre and Petit [14] and Lin and Armfield [15], all of which considered unsteady effects. A steady numerical simulation, along with experimental work in a vertical cylinder with internal heat generation has also been presented by Holzbecher and Steif [16]. Apart from

* Corresponding author. Tel.: +30-1-650-3817; fax: + 30-1-654-4592.

E-mail address: elpapa@mail.demokritos.gr (E. Papanicolaou).

0017-9310/02/$ - see front matter © 2002 Published by Elsevier Science Ltd.
PII: S0017-9310(01)00258-7

Nomenclature

A	aspect ratio of the enclosure $A = L/D$
D	diameter of the enclosure (m)
Fo	Fourier number $Fo = \alpha t/LD$
g	magnitude of the gravitational acceleration (m/s^2)
Gr	Grashof number $Gr = g\beta\Delta TL^3/v^2$
h	local heat transfer coefficient along the heated surface (W/m^2K)
k	turbulent kinetic energy non-dimensionalized by $(v/L)^2$
L	total height of the enclosure (m)
$\overline{Nu}_w$	average Nusselt number over the heated surface $\overline{Nu}_w \int_0^1 (1/\theta_w)\,dZ$
Nu_z	local Nusselt along the heated surface $Nu_z = hz/\lambda = (1/\theta_w)Z$
Pr	Prandtl number of water $Pr = v/\alpha$
q''_w	heat flux per unit heated surface area (W/m^2)
Ra	Rayleigh number $Ra = Gr \times Pr = g\beta\Delta TL^3/v\alpha$
r', z	radial and axial coordinate distances, respectively (m)
r, Z	dimensionless radial and axial coordinate distances, respectively, $r = r'/L$, $Z = z/L$
t	physical time (s)
T	local temperature (K)
$u_r,\ u_z$	radial and axial velocity components, respectively (m/s)
$U_r,\ U_z$	dimensionless velocity components $(U_r,\ U_z) = (u_r/(v/L),\ u_z/(v/L))$

Greek symbols

α	thermal diffusivity of water (m^2/s)
α_t	eddy diffusivity for heat
β	coefficient of thermal expansion of water $\beta \equiv -(1/\rho)(\partial\rho/\partial T)_p$ (K^{-1})
ΔT	temperature scale $\Delta T = q''_w L/\lambda$
ϵ	rate of dissipation of the turbulent kinetic energy, non-dimensionalized by v^3/L^4
θ	dimensionless temperature $\theta = (T - T_i)/\Delta T$
λ	thermal conductivity of water (W/m K)
v	kinematic viscosity of water (m^2/s)
v_t	turbulent viscosity
$\sigma_k,\ \sigma_\epsilon$	Prandtl number for the turbulent kinetic energy and its rate of dissipation, respectively
σ_t	turbulent Prandtl number $\sigma_t = v_t/\alpha_t$
τ	dimensionless time $\tau = t/(L^2/v)$
τ_w	wall shear stress (N/m^2)
Ψ	dimensionless stream function $U_r = -\frac{1}{r}\partial\Psi/\partial Z$, $U_z = \frac{1}{r}\partial\Psi/\partial r$
Ω	dimensionless vorticity $\Omega = \Omega_\theta = \partial U_r/\partial Z - \partial U_z/\partial r$

Subscripts

i	initial value
w	value of a variable at the wall
∞	value at the core of the enclosure

completely enclosed tanks or vessels, a few studies have dealt with enclosures with openings, through which a fluid of different temperature enters or exits, i.e., with the mixed convection problem [17–19].

Almost all the aforementioned numerical studies have dealt with laminar flow simulations. Only Evans et al. [5] have attempted an analytical treatment of the turbulent boundary layer along the heated wall using an integral method, while Holzbecher and Steif [16] have used an elliptic, commercially available code for steady, turbulent-flow computations. Although when dealing with the relevant practical applications, such as thermal storage mentioned above, a question that often arises is whether to employ a laminar- or turbulent-flow simulation, the relevant work up to the present date on vertical cylinders has not yet provided concrete evidence as to where each of the two approaches should be adopted. Specifically in terms of a critical value (or a range of values) of the Rayleigh number that determine the limits of each flow regime (upper limit for laminar, lower limit for turbulent flow). This study attempts to investigate this intermediate area and explore the performance of several turbulence models for the full elliptic numerical simulation of such problems in cylindrical configurations. There are certainly several combinations of geometric parameters and boundary conditions that can be specified, as the aforementioned literature review shows, for instance, heating (or cooling) can be provided from the cylindrical or the flat surfaces (or both), at constant temperature or constant heat flux etc.

There will definitely be a need to eventually study several alternative cases and attempt to relate the findings in order to obtain some universally applicable theory. However, the scope of this study cannot cover such a broad spectrum and will deal with a representative case, an approach which is nevertheless sufficient for the sake of presenting a methodology based on which other configurations may be treated. Therefore, in the present study the natural convection in a vertical cylinder heated from its lateral surface has been considered as a good representative case, as there are relevant experimental results available [5,6]. Besides, as pointed out by Hyun [20], who analyzed the development of stratification in a

initially homogeneous cylindrical enclosure after applying a vertical temperature gradient along the vertical wall at $t = 0$, the study of such unsteady processes attained by constant-heat-flux heating has been very limited. This is more so at high Rayleigh numbers and the present work aims at providing new evidence along these lines, particularly by using turbulence models in an elliptic unsteady numerical formulation and dealing with the development of stratification and how this interacts with turbulence.

2. Mathematical model

2.1. Model equations

The configuration under investigation is shown in Fig. 1. The equations describing continuity and conservation of momentum and energy in axisymmetric configurations such as the present one, can be written in the stream function–vorticity formulation and for turbulent flow (where the overbars denote mean velocities obtained after Reynolds averaging of the momentum equations) as:

- Continuity

$$\frac{\partial \overline{U}_r}{\partial r} + \frac{\partial \overline{U}_z}{\partial Z} = -\frac{\overline{U}_r}{r}. \tag{1}$$

- Stream function

$$\frac{\partial}{\partial r}\left(\frac{1}{r}\frac{\partial \Psi}{\partial r}\right) + \frac{1}{r}\frac{\partial^2 \Psi}{\partial Z^2} = -\Omega. \tag{2}$$

- Vorticity

$$\frac{\partial \Omega}{\partial \tau} + \frac{\partial}{\partial r}\left[\overline{U}_r \Omega - \Gamma_\Omega \frac{\partial \Omega}{\partial r}\right] + \frac{\partial}{\partial Z}\left[\overline{U}_z \Omega - \Gamma_\Omega \frac{\partial \Omega}{\partial Z}\right] = \underbrace{-C_B \frac{\partial \theta}{\partial r}}_{\text{Buoyancy term}} + \underbrace{\Gamma_\Omega \frac{\partial}{\partial r}\left(\frac{\Omega}{r}\right)}_{\text{Curvature term 1}} - \underbrace{\Gamma_\Omega \frac{\partial}{\partial r}\left(\frac{\tau^t}{r}\right)}_{\text{Curvature term 2}} + \Gamma_\Omega\left(\frac{\partial^2 \tau^t}{\partial r^2} - \frac{\partial^2 \tau^t}{\partial Z^2}\right) - \Gamma_\Omega\left(\frac{\partial^2 \zeta^t}{\partial r \partial Z}\right). \tag{3}$$

- Energy

$$\frac{\partial \theta}{\partial \tau} + \frac{\partial}{\partial r}\left[\overline{U}_r \theta - \Gamma_\theta \frac{\partial \theta}{\partial r}\right] + \frac{\partial}{\partial Z}\left[\overline{U}_z \theta - \Gamma_\theta \frac{\partial \theta}{\partial Z}\right] = -\frac{1}{r}\left(\overline{U}_r \theta - \Gamma_\theta \frac{\partial \theta}{\partial r}\right). \tag{4}$$

In the present case, where v/L is used as the velocity scale, and with $v_t^* = v_t/v$

$$\Gamma_\Omega = 1, \quad C_B = \frac{Ra}{Pr}, \quad \Gamma_\theta = \Gamma_\Omega\left(\frac{1}{Pr} + \frac{v_t^*}{\sigma_t}\right).$$

In the vorticity equation the Boussinesq approximation has been used. The first curvature term is present in

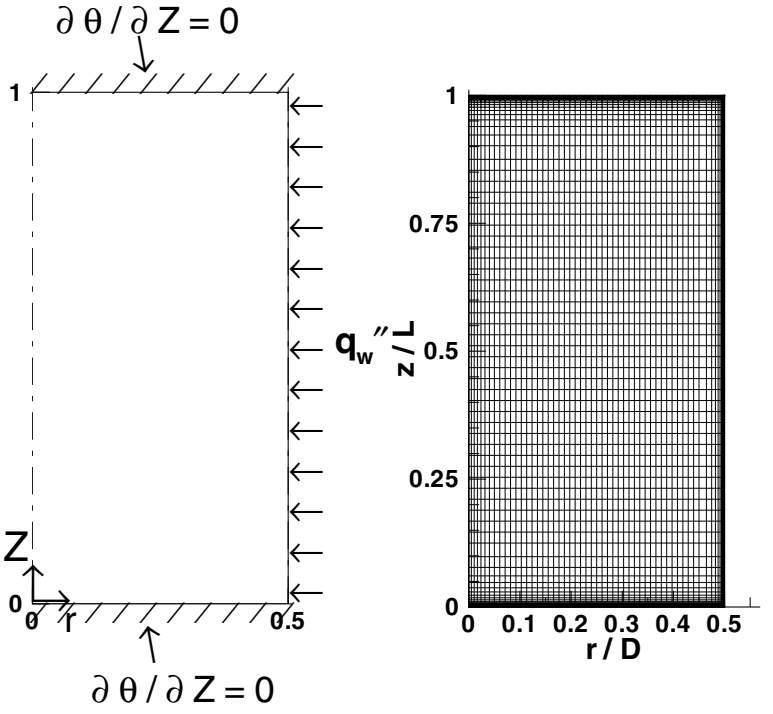

Fig. 1. Enclosure configuration with the boundary conditions and computational grid.

both laminar and turbulent flows, whereas the second one only in turbulent flow. The Reynolds stress terms and the turbulent heat fluxes, following the Bousinessq eddy viscosity concept, have been taken as:

$$-\overline{u_i'u_j'} = \Gamma_\Omega \nu_t^* \left(\frac{\partial \overline{U}_j}{\partial X_i} + \frac{\partial \overline{U}_i}{\partial X_j}\right) - \frac{2}{3}k\delta_{ij},$$
$$-\overline{u_i'\theta'} = \frac{\nu_t^*}{\sigma_t}\left(\frac{\partial \theta}{\partial X_i}\right), \tag{5}$$

where X_i, $X_j = (r, Z)$ and u_r', u_z' are the velocity fluctuations in the radial and axial directions, respectively. In the last two terms of Eq. (3), which arise from the Reynolds stresses, the following quantities have been defined:

$$\tau' = \nu_t^*\left(\frac{\partial \overline{U}_z}{\partial r} + \frac{\partial \overline{U}_r}{\partial Z}\right), \quad \varsigma' = 2\nu_t^*\left(\frac{\partial \overline{U}_z}{\partial Z} - \frac{\partial \overline{U}_r}{\partial r}\right) \tag{6}$$

For the k–ϵ model, which is used in the present study, the transport equations for k and ϵ are written as:

- Turbulent kinetic energy

$$\frac{\partial k}{\partial \tau} + \frac{\partial}{\partial r}\left[\overline{U}_r k - \Gamma_k \frac{\partial k}{\partial r}\right] + \frac{\partial}{\partial r}\left[\overline{U}_z k - \Gamma_k \frac{\partial k}{\partial Z}\right]$$
$$= \underbrace{-\frac{1}{r}\left(\overline{U}_r k - \Gamma_k \frac{\partial k}{\partial r}\right)}_{\text{Curvature term}} + P_k + G_k - \epsilon + D_k. \tag{7}$$

- Dissipation rate of turbulent kinetic energy

$$\frac{\partial \epsilon}{\partial \tau} + \frac{\partial}{\partial r}\left[\overline{U}_r \epsilon - \Gamma_\epsilon \frac{\partial \epsilon}{\partial r}\right] + \frac{\partial}{\partial r}\left[\overline{U}_z \epsilon - \Gamma_\epsilon \frac{\partial \epsilon}{\partial Z}\right]$$
$$= \underbrace{-\frac{1}{r}\left(\overline{U}_r \epsilon - \Gamma_\epsilon \frac{\partial \epsilon}{\partial r}\right)}_{\text{Curvature term}} + C_1 f_1 P_k \frac{\epsilon}{k} + C_3 G_k \frac{\epsilon}{k}$$
$$- C_2 f_2 \frac{\epsilon^2}{k} + E_\epsilon, \tag{8}$$

where in the present case $\Gamma_k = \Gamma_\epsilon = 1$ and the viscosity ratio ν_t^* and the production terms of the turbulent kinetic energy due to shear P_k and buoyancy G_k are given by the following expressions:

$$\nu_t^* = \Gamma_\Omega f_\mu C_\mu \frac{k^2}{\epsilon}, \tag{9}$$

$$P_k = \nu_t^*\left[2\left(\frac{\partial \overline{U}_r}{\partial r}\right)^2 + \left(\frac{\partial \overline{U}_z}{\partial r} + \frac{\partial \overline{U}_r}{\partial Z}\right)^2 + 2\left(\frac{\partial \overline{U}_z}{\partial Z}\right)^2 + 2\left(\frac{\overline{U}_r}{r}\right)^2\right],$$

$$G_k = -\frac{Ra}{Pr}\frac{\nu_t^*}{\sigma_t}\frac{\partial \theta}{\partial r}. \tag{10}$$

The constants have typically the following values: $C_\mu = 0.09$, $C_1 = 1.44$, $C_2 = 1.92$, $\sigma_k = 1.0$ and $\sigma_\epsilon = 1.3$. Deviations from this set of values will be described below, where they occur. For C_3 the following expression is used: $C_3 = \tanh|U_z/U_r|$ [4]. The value of the turbulent Prandtl number is taken as constant throughout this study, equal to $\sigma_t = 0.9$. The damping functions f_μ, f_1, f_2 and the terms D_k, E_ϵ, differ for each turbulence model used and their form will be described below.

2.2. Boundary conditions

The thermal boundary conditions are shown in Fig. 1. The constant-heat-flux condition gives: $\partial\theta/\partial r = -1$ at the wall. The stream function is set to zero at the walls, which leads to zero values for both velocity components, whereas the wall vorticity is computed from the stream-function values in the direction normal to the wall [21], after performing suitable Taylor series approximations. For the turbulence variables, the wall values used depend on the corresponding turbulence model, as will be outlined below. On the axis of the enclosure ($r = 0$), $\psi = \Omega = U_r = 0$, whereas the r-derivatives of θ, U_z, k and ϵ are set to zero.

2.3. Turbulence models

In this work, several low-Reynolds models as well as the two-layer model [22] are used to simulate the turbulence effects. The standard k–ϵ turbulence model with the wall function approach [23] has not been found to be adequate to model natural convective flows and heat transfer, unless modified wall functions are used [21]. It has, however, been used here only for specific comparisons, as will be explained below, in the form suggested by Henkes and Hoogendoorn [4], which allows for placing the first grid point very close to the wall, using $\epsilon_w = large$, thus providing adequate resolution of the velocity boundary layer. The low-Reynolds models used are those by Launder and Sharma (LS) [24], Chien (CH) [25], Abe, Kondoh and Nagano (AKN) [26] and Lam and Bremhorst (LB) [27]. The various functions involved in these models are shown in Table 1, where $y^+ = u_\tau y_n/\nu$, $y^* = \sqrt{k}y_n/\nu$, $Re_t = k^2/\nu\epsilon$, y_n is the distance normal to the wall and $u_\tau = \sqrt{\tau_w/\rho}$ is the friction velocity. [1] The AKN model is particularly suited for recirculating flows since it makes use of the Kolmogorov velocity scale $u_\epsilon = (\nu\epsilon)^{1/4}$ instead of the friction velocity u_τ, which is singular at separation and reattachment points. Therefore in this model, $y^* = u_\epsilon y_n/\nu$ is used to define the functions in Table 1. The functions D_k, E_ϵ are zero for all

[1] All these parameters are presented here in their standard dimensional form, as encountered in the literature, even though they are used after suitable non-dimensionalization in the present work.

Table 1
Functions for the chosen low-*Re* turbulence models

Model	f_μ	f_1	f_2
LS	$\exp\left[\frac{-3.4}{(1.0+Re_t/50)^2}\right]$	1.0	$1.0-0.3\exp(-Re_t^2)$
CH	$1-\exp(-0.0115y^+)$	1.0	$1.0-0.22\exp[-(Re_t/6)^2]$
AKN	$\left\{1-\exp\left(-\frac{y^*}{14}\right)\right\}^2 \times\left[1+\frac{5}{Re_t^{3/4}}\exp\left\{-\left(\frac{Re_t}{200}\right)^2\right\}\right]$	1.0	$\left\{1-\exp\left(-\frac{y^*}{3.1}\right)\right\}^2 \times\left[1-0.3\exp\left\{-\left(\frac{Re_t}{6.5}\right)^2\right\}\right]$
LB	$[1-\exp(-0.0165y^*)]^2\times\left(1+\frac{20.5}{Re_t}\right)$	$1.0+\left(\frac{0.05}{f_\mu}\right)^3$	$[1.0-0.27\exp(-Re_t^2)] \times[1.0-\exp(-y^*)]$

models but the CH, where they have the following values (in dimensional form):

$$D_k=-2\nu\frac{k}{y_n^2},\quad E_\epsilon=-2\frac{\nu\epsilon}{y_n^2}\exp(-0.5y^+). \tag{11}$$

At the wall, the CH model takes $k=\epsilon=0$, whereas in the LS, AKN and LB models the following conditions are specified:

$$k_w=0,\quad \epsilon_w=2\nu\left(\frac{\partial\sqrt{k}}{\partial y_n}\right)=2\nu\frac{k_1}{y_{n1}^2}, \tag{12}$$

where k_1, y_{n1} are, respectively, the values of k and the wall distance at the first point from the wall. The AKN model constants that differ from the standard values mentioned above are: $C_1=1.5$, $C_2=1.9$, $\sigma_k=1.4$ and $\sigma_\epsilon=1.4$. The CH model also slightly differs by specifying: $C_1=1.35$, $C_2=1.8$. In the LB model, the form for f_2 proposed by Davidson [28] is used, which behaves better in laminar flow regions where Re_t is very low. The two-layer model used here (TL) is in the form proposed by Xu et al. [29], which employs DNS data for natural convection in order to model the near-wall region and the standard k–ϵ in the outer region. It uses the square root of the wall-normal stress $\overline{v'v'}$ as the velocity scale instead of $\sqrt{k}$. This is obtained by the following relation:

$$\frac{\overline{v'v'}}{k}=7.19\times10^{-3}y^*-4.33\times10^{-5}y^{*^2}+8.8\times10^{-8}y^{*^3}, \tag{13}$$

while the viscosity and the dissipation scales are, respectively, given by

$$l_\mu=\frac{0.544y_n}{1+5.025\times10^{-4}y_v^{*1.65}},\qquad l_\epsilon=\frac{8.8y_n}{1+10/y_v^*+5.15\times10^{-2}y_v^*}, \tag{14}$$

where $y^*=\sqrt{k}y_n/\nu$ and $y_v^*=\sqrt{\overline{v'v'}}y_n/\nu$.

3. Numerical scheme

3.1. General features

The numerical scheme used has been described by Papanicolaou and Jaluria [21]. The discretized, time-dependent transport equations are integrated over non-overlapping finite volumes, with the ADI method being used for the time marching. The linear systems thus obtained are solved using the TDMA algorithm. The convective terms in the vorticity and energy equations are here discretized using the higher-order, bounded HLPA scheme described by Zhu [30], while the power-law scheme is used for the turbulence variables. The stream-function equation is solved by the successive over-relaxation method (SOR). The wall vorticity is computed by a first-order formula [21] which is more stable and readily applicable to non-uniform grids.

3.2. Validation

For validation in the case of laminar natural convection, the experimental results of Hess and Miller [6] for a vertical cylinder were used, as will be described below. For turbulent natural convection, due to lack of standard experimental results for cylindrical enclosures, all turbulence models used in the present code were validated against the more established, for the sake of comparisons with computations, set of experimental data obtained by Cheesewright et al. [31] for rectangular geometries. A differentially heated cavity of aspect ratio $A=5$ was considered and values of all significant quantities were measured at different locations within the cavity. Computed results from the five different turbulence models used in the present computer code at $Ra_H=5\times10^{10}$ and for a 60×60 grid are shown in Fig. 2. The velocity profiles at mid-height are shown to be captured well by all models (Fig. 2(a)). Discrepancies

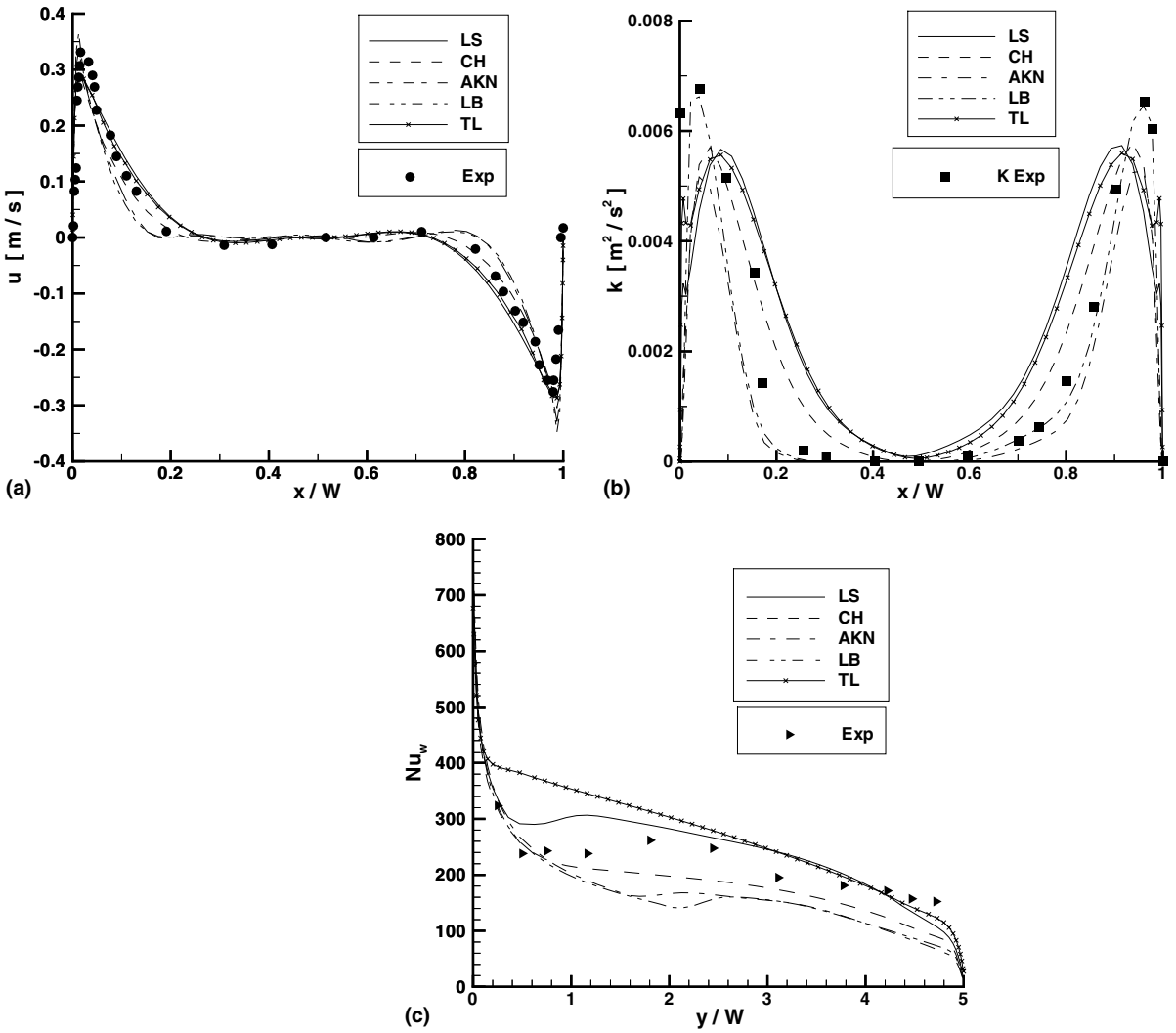

Fig. 2. Comparison of turbulent flow results obtained with different models against experiments [31]. The latter are for natural convection in a differentially heated rectangular cavity of aspect ratio 5 (height to width) at $Ra_H = 5 \times 10^{10}$. (a) Vertical velocity profiles; (b) turbulent kinetic energy; (c) hot wall Nusselt number.

occur in the prediction of the turbulent kinetic energy (Fig. 2(b)) and the Nusselt number along the heated wall (Fig. 2(c)). The AKN model approaches the experimental curve of k better than the other models, for the most part, but the Nusselt number curve is better approached by the Chien and the Launder–Sharma models, the latter of which exhibits a more distinct transition pattern, almost at the right location.

3.3. Computational grid

Computations have been performed by successively increasing the grid dimensions and considering values of 30×60, 60×60, 60×80 and 90×120 (radial $\times$ axial directions). It was found that the 60×80 grid provided a good compromise as the base grid between the computational effort needed to simulate transient flow without resorting to extremely small time steps on one hand and accuracy on the other hand. Minor differences have been observed between the chosen grid and the higher dimension of 90×120, to be further discussed below. The form of the base grid is shown in Fig. 1. The grid was made finer towards the walls, especially towards the heated one and smaller stretching had to be used towards the axis, in order to adequately capture the downward motion of the hot fluid and the secondary flows that were found to develop near the axis.

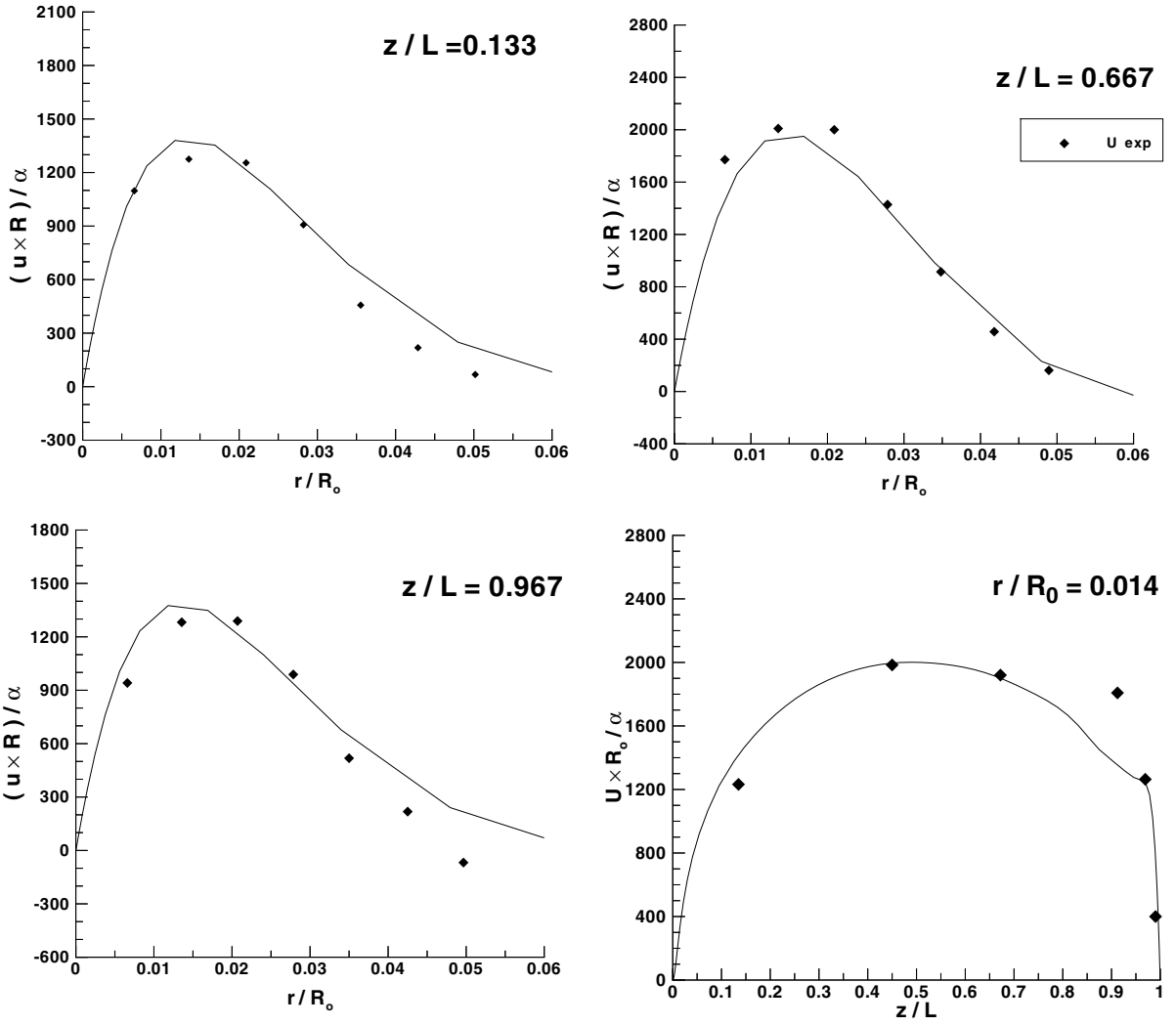

Fig. 3. Comparisons of computed velocity profiles in the boundary layer (solid lines) with the experimental data (points) of Hess and Miller [6] in the quasi-steady regime for $Ra = 2.5 \times 10^{10}$.

4. Results and discussion

4.1. Theoretical background

The physical phenomena taking place and mechanisms present during the transient state inside a cylindrical enclosure subject to a sudden change in boundary conditions at time $t = 0$ have been analyzed by previous investigators [5,15,20]. A thermal boundary layer develops initially along the heated wall(s), followed by a stratification process gradually developing from top to bottom for the heat-up, or bottom to top if the fluid is being cooled (cool-down). Estimates for the time scales of the completion of these two processes have also been presented. For a fluid heated or cooled isothermally from the side wall and/or the bottom surface, steady thermal and flow fields are eventually attained. For constant-heat-flux heating at the wall and adiabatic horizontal boundaries, the flow field will eventually reach a steady state, but the thermal field will constantly be developing as long as there is heat input to the fluid. Therefore, this situation can be described as *quasi-steady*.

Although several studies have addressed this problem, focusing on Rayleigh numbers typical of laminar flow, very little is known on the behavior of the system at high Rayleigh numbers, characteristic of turbulent flow. The most relative information that can be used as a guide comes from previous experimental and analytical studies on flat vertical surfaces, in which the transition

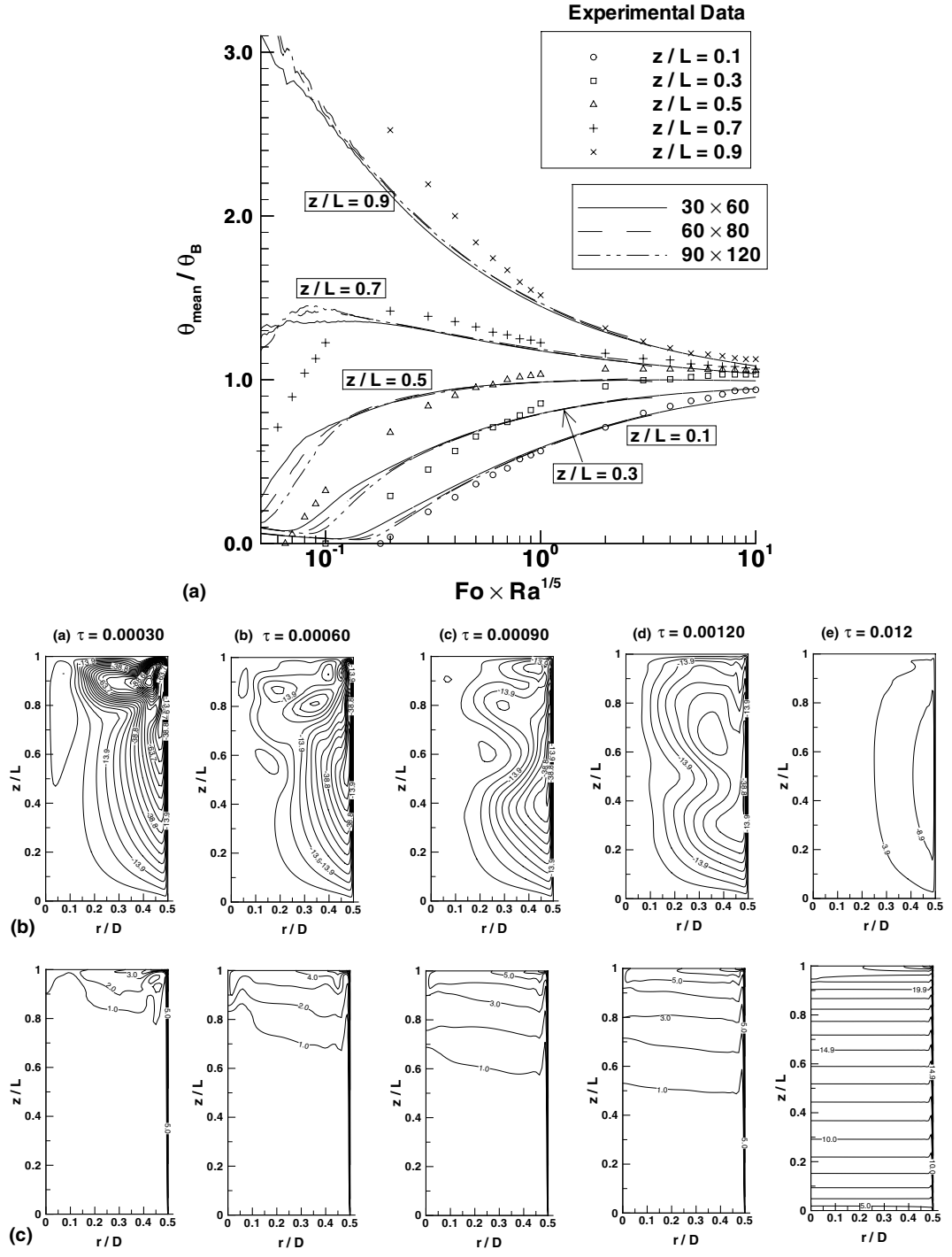

Fig. 4. Computed laminar flow results for $L/D = 1$, $Ra = 10^{12}$. (a) Transient mean temperatures over horizontal planes (lines) vs. approximated experimental data [5], including the effect of the grid dimensions. (b) Streamlines and (c) isotherms ($\theta \times 10^3$) at times corresponding to $Fo \times Ra^{1/5} = 0.0254$, 0.0508, 0.07625, 0.1017 and 1.017.

to turbulence for a natural convection boundary layer heated at a constant heat flux was considered. These studies have found that transition occurs at a higher value of the Rayleigh number compared to an isothermal surface. More specifically, whereas for an isothermal surface transition for air starts at a Rayleigh

number of order 10^9, for a constant-heat-flux surface this occurs at an order of 10^{11} [32]. For water, the studies of Vliet and Liu [33] and Qureshi and Gebhart [34] have found an even higher value. Ref. [34] has proposed a range of $Ra = 1.2 \times 10^{13}$–4×10^{13} for the start of transition and $Ra = 5 \times 10^{13}$–10^{14} for its completion. In the present problem, such values can certainly be used as a hint in an effort to examine the high-Ra regime, however, it is to be kept in mind that there are two additional factors that are expected to affect the present behavior, namely, the surface curvature and the thermal stratification of the core of the fluid in the enclosure. Therefore, a departure from the documented transition criteria can be expected. In particular, the effect of stratification is more well known and is expected to act towards destroying turbulence and laminarizing the flow.

4.2. Laminar flow

4.2.1. Quasi-steady velocity field

Due to a lack of experimental velocity-field data in the turbulent flow regime for this problem, the results for rectangular cavities [31] have been used for comparisons, as discussed earlier, while for cylindrical geometries suitable experimental results were only found in the high-Ra, laminar flow regime, obtained by Hess and Miller [6]. They used a Laser–Doppler velocimeter in their measurements, in a vessel of aspect ratio $L/D = 0.95$ containing water. The computed vertical velocity in the boundary layer is compared in Fig. 3 in the quasi-steady flow regime, for $Ra = 2.5 \times 10^{10}$. Since in the experiment the cylindrical vessel was not completely full but the water had a free surface, the boundary condition used here at the top was that for an adiabatic surface that allowed slip. The grid used in this particular case was 60×60, while the Prandtl number was $Pr = 5.388$, corresponding to 30 °C and, thus, approximating the experimental conditions.

4.2.2. Transient thermal field

The variation of the temperature field with time is compared against existing experimental results compiled by Evans et al. [5] in Fig. 4(a). The curves represent an approximation of data obtained in vertical cylinders for a variety of heating rates, aspect ratios and fluids. Time histories of normalized mean temperatures at five selected horizontal planes are plotted

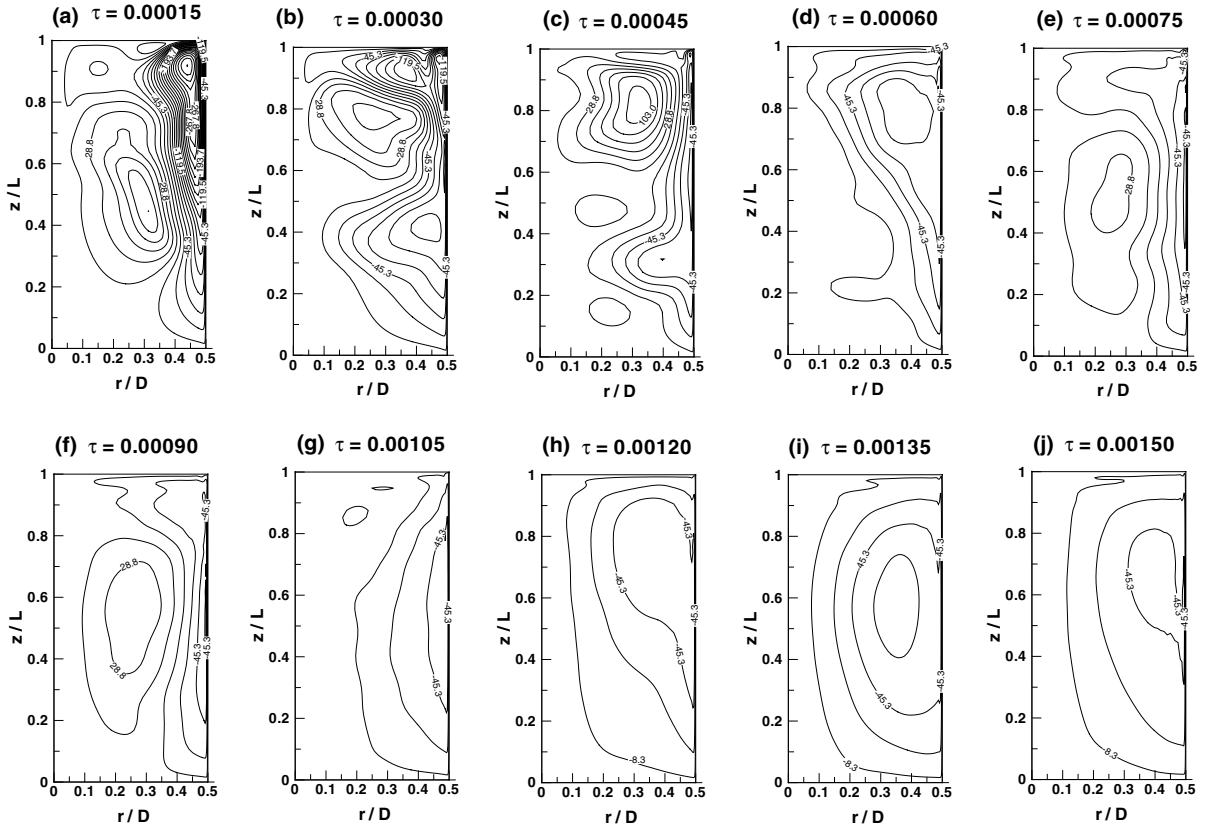

Fig. 5. Streamlines computed at various time instants, for $Ra = 5 \times 10^{13}$ using the AKN model, $\Psi_{\min} = -342$, $\Psi_{\max} = 103$.

against a dimensionless time parameter. The normalization value θ_B is the bulk temperature, i.e., the temperature that would prevail in the enclosure if the fluid were perfectly mixed at each time. The curves obtained by the present computations are for $L/D = 1$, $Ra = 10^{12}$ and for $Pr = 2.965$ (60 °C), which lies closer to the experiments of Evans et al. [5] for water. Although the general form of the experimental curves is captured well, there appears to be a discrepancy at the early transients but this becomes smaller after an abscissa value of approximately 0.2–0.3. After more carefully observing the curves presented in [5] however, the impression given is that the part corresponding to $Fo \times Ra^{1/5} \leqslant 0.2$ is obtained based on a much scarcer set of data than the subsequent part, which can, therefore, be considered as better representing the general behavior. At large times, discrepancies remain for the locations $z/L = 0.3$ and 0.5. However, the experimental data for both these locations at large times seem to exceed the value of 1, expected to prevail eventually at $z/L = 0.5$, whereas in the computed results this value is approached from below with a fairly good accuracy, being equal to 0.998 at $z/L = 0.5$. The effect of the grid dimensions is also shown. Interestingly enough, the grids exhibit differences only at the early stages, up to $Fo \times Ra^{1/5} = 0.1$–0.2, but then all three of them almost collapse to the same curve at each respective height. In Figs. 4(b and c) streamlines and isotherms are presented for the same configuration at different time instants, mostly during the early transient before the enclosure becomes fully stratified and when there is significant secondary flow activity.

4.3. Turbulent flow

4.3.1. Input parameters

Up to $Ra = 10^{13}$ laminar results could be obtained, however, as discussed in the beginning of this section and after considering the flat-plate findings [33,34], turbulent flow should be expected for $Ra \geqslant 5 \times 10^{13}$. The turbulence models were therefore first employed for $Ra = 5 \times 10^{13}$ and the computations continued by increasing the Rayleigh number in small steps, successively to $Ra = 10^{14}$, 2.5×10^{14}, 4×10^{14} and 10^{15}. After the latter value, convergence was difficult to achieve. Besides, at higher values it becomes questionable whether the very thin boundary layers that develop can be adequately resolved with the same grid. In order to

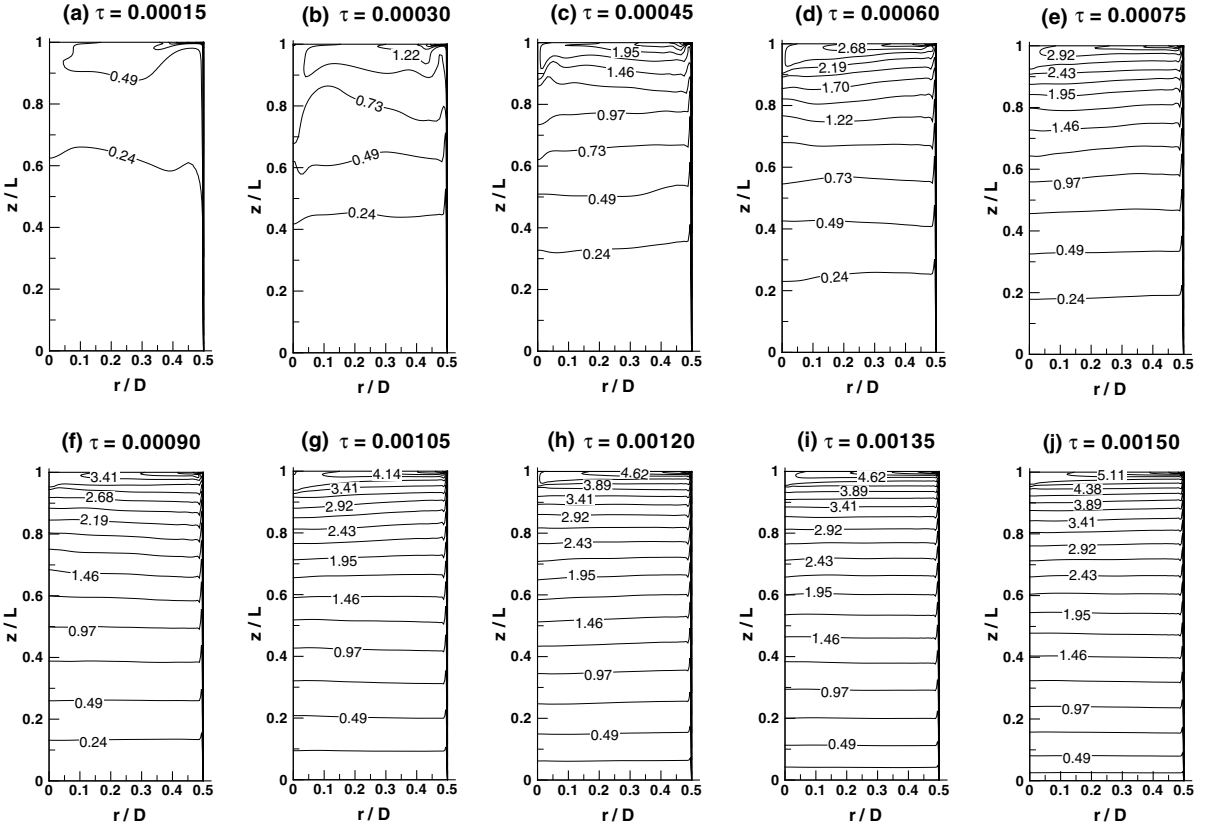

Fig. 6. Isotherms computed at various time instants, for $Ra = 5 \times 10^{13}$ using the AKN model, $\theta_{max} \times 10^3 = 7.34$.

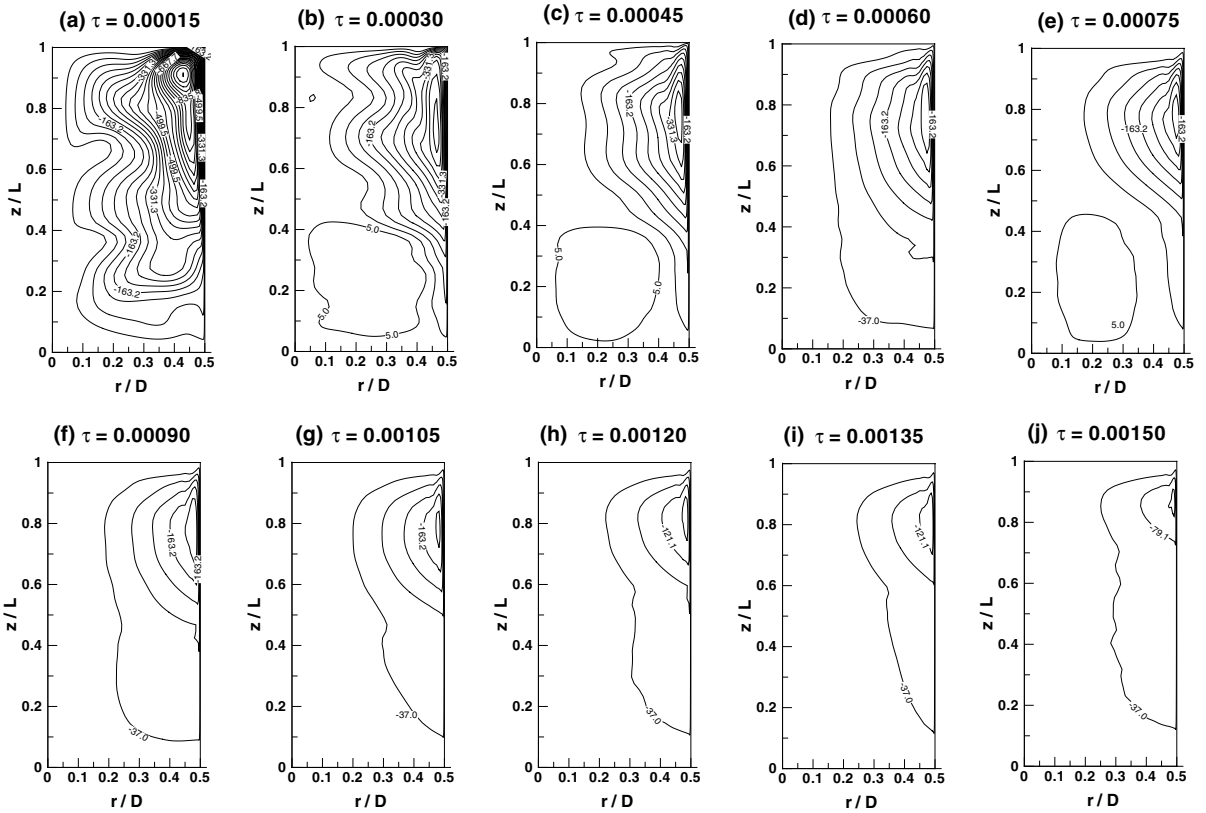

Fig. 7. Streamlines computed at various time instants, for $Ra = 10^{15}$ using the AKN model, $\Psi_{\min} = -1004$, $\Psi_{\max} = 5$.

obtain reasonable time steps and computation times, and since the allowable maximum value of the time step is limited by the minimum distance of the first grid point from any wall, the first point from the heated wall was set at a fixed distance of 1.8×10^{-4}. A distance of this magnitude was found to yield at least four nodes between the maximum velocity in the boundary layer and the wall in square-cavity simulations [4], as was also the case here. With this value the maximum allowable time step was $\Delta\tau = 3 \times 10^{-8}$ but as the value of Ra increases and the boundary layer becomes thinner, it can no more be adequately resolved with the same grid spacing. By further decreasing the distance of the first grid point to the wall, the time step has to be reduced in a quadratic fashion, making the increase in computational effort very steep. Therefore, it was decided not to proceed to higher values of Ra then 10^{15}, considering also that the expected range of Ra in relevant practical applications has been covered to an adequate extent.

Computations proceeded until the flow field reached a steady state, for which 150,000–200,000 time steps were needed ($\tau = 4.5$–6×10^{-3}), depending on the value of Ra. To initialize the turbulence variables, a turbulence level of 1% was assumed and therefore the turbulent kinetic energy, in accordance with the practice in forced flow problems, should be taken equal to $0.01^2 \times U_{\text{ref}}^2$, where U_{ref} is a suitable reference velocity. Due to lack of a characteristic velocity (such as inlet or free-stream) in the present natural convection problem to yield a reference value, use of the buoyancy velocity $u_{\text{b}} = \sqrt{g\beta\Delta\overline{T}L}$ was made and specifically $U_{\text{ref}} = 0.1U_{\text{b}}$ was found to be a good choice. For the rate of dissipation, a length scale $l_\epsilon = 0.03 \times (D/2)$ was chosen and the initial value of the turbulent viscosity was obtained from the expression of Eq. (9). Typical CPU times in seconds per time step required for the 60×80 grid on a Pentium III, 600-MHz processor were: 0.339 for the LS model, 0.349 for CH, 0.363 for AKN, 0.367 for LB, 0.348 for TL and 0.329 for the standard k–ϵ model.

Up to a time period equal to $\tau = 1.5 \times 10^{-3}$, i.e. 50,000 time steps, changes are more rapid and for all low-Re models the process of an initial boundary layer transition and relaminarization, which has been observed, has already been completed. Therefore results for the flow and thermal fields, wall heat transfer and heated wall temperature distribution are sampled at a higher frequency within this period, more specifically, at intervals of $\Delta\tau = 1.5 \times 10^{-4}$. Afterwards, the sampling is less frequent, at $\Delta\tau = 6.0 \times 10^{-4}$. In this time period, even though the low-Re models predict laminarization,

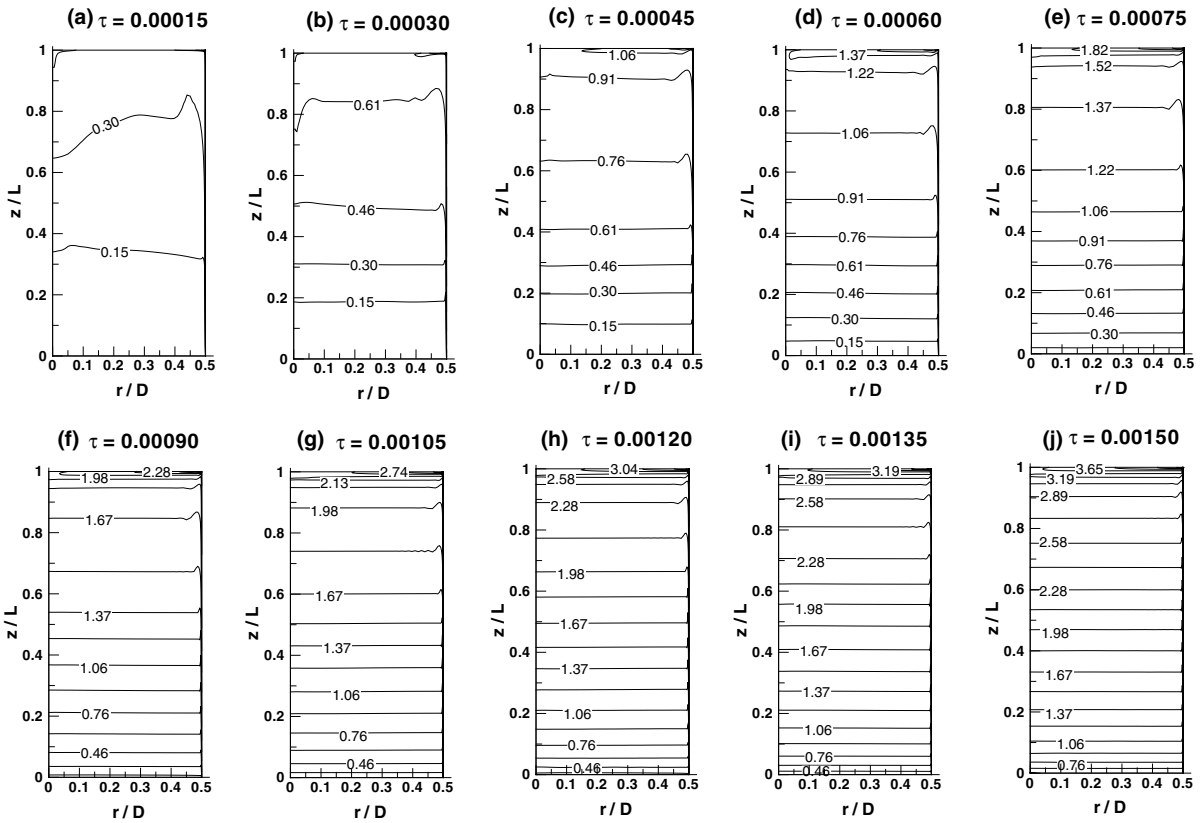

Fig. 8. Isotherms computed at various time instants, for $Ra = 10^{15}$ using the AKN model, $\theta_{max} \times 10^3 = 4.56$.

it should be noted that the fluid has already undergone a mixing process, much larger than would have been the case should the flow had remained laminar at all times. Consequently, the development of the thermal field after relaminarization has taken place is different than would have been the case for a flow that would have been laminar at all times.

4.3.2. Flow and thermal fields

The flow and thermal fields at the selected time instants within $\tau = 1.5 \times 10^{-3}$, as explained above, and for the two limiting values of *Ra* used in the turbulent flow simulations, i.e., $Ra = 5 \times 10^{13}$ and 10^{15}, are shown in Figs. 5–8. All these are results of computations that employed the AKN model. Both Figs. 5 and 7 reveal a large degree of activity as far as secondary flows in the enclosure are concerned. After a certain time, which is shorter the higher the Rayleigh number as can be deduced by comparing the two figures, the secondary flow activity is being reduced and the flow field approaches a quasi-steady state. The development of stratification can be observed in Figs. 6 and 8. Both the heated-wall boundary layer and the mixing zone at the top can be seen to gradually become thinner with time. After the last results shown, for $\tau = 1.5 \times 10^{-3}$, the qualitative features do not change considerably.

The development of turbulence, as predicted by the various models, can be observed in Fig. 9, where contour plots of the turbulent viscosity ν_t^* are shown at different time instants for $Ra = 10^{14}$. Although this is at a different value of *Ra* than the previous figures, it should be noted that qualitatively the picture is very similar for the other values of *Ra* as well. The different behavior between a low-*Re* model such as the AKN model, whose results are shown on top and the TL model shown on bottom becomes obvious. At this value of *Ra*, the AKN model predicts relaminarized flow already at $\tau = 7.5 \times 10^{-4}$, whereas the TL model predicts sustained turbulence. The form of the turbulent viscosity field predicted by the TL model does not change significantly with time, but its maximum value maintains a very small rate of decrease.

Over the range of *Ra* considered, all low-*Re* turbulence models have exhibited a behavior similar to the one presented in Fig. 9, i.e., at first a transition from laminar to turbulent boundary layer along the heated wall, as will be further discussed later, with a turbulent-flow region developing at the upper half of the heated

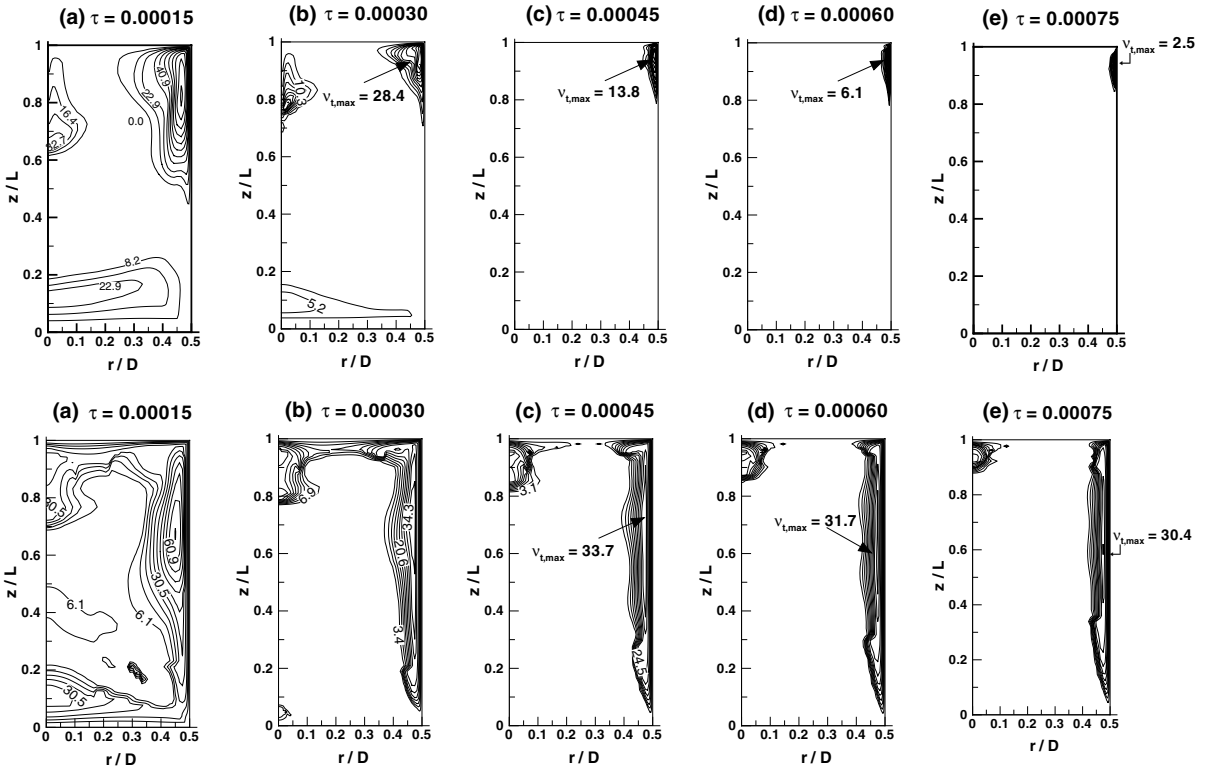

Fig. 9. Contours of viscosity ratio ν_t^* at different times, computed by the AKN (top) and TL (bottom) models for $Ra = 10^{14}$.

wall initially ($\tau \leqslant 7.5 \times 10^{-4}$). These times corresponded to the boundary layer regime [20]. The location of the transition point from a laminar to a turbulent boundary layer was found to vary with each model. Gradually, as stratification of the fluid in the cylinder started to develop, the turbulent flow region was shifted upwards, towards the upper right corner and its size shrunk. With the increase in the value of Ra up to 10^{15} only a delay in relaminarization was found and it did nevertheless occur at later times. The different behavior of the TL model, which predicted sustained turbulence, could be explained by the fact that this model employs a high-Re form which does not make use of any damping functions in the region far from the wall, while on the other hand it does not include the effect of buoyancy on dissipation rate in the near-wall region, although this is taken into account in the k equation. In fact, in order to further investigate the high-Re modelling effect further, simulations with the SKE model have been performed at $Ra = 10^{14}$, in the form used in the benchmark computations of turbulent flow in a square cavity [4] and the results obtained did exhibit a similar behavior as the TL model.

Previous attempts to simulate turbulent flow in vertical cylinders using low-Re k–ϵ models, albeit in different configurations [16], have found the flow to be laminar at $Ra = 5 \times 10^{13}$ and had to introduce an additional production term in the turbulent kinetic energy equation in order to obtain turbulent flow, as observed in the experiments. However, the aforementioned simulation was steady and did not provide details of the transient state. Here it is observed that, even though the low-Re models do not predict sustained turbulence in the enclosure at large times for all Rayleigh numbers considered, there is however a transient period, of varying duration, which exhibits the characteristics of turbulent flow. More specifically, of a laminar-to-turbulent transition of the natural convection boundary layer, followed by a gradual relaminarization, as stratification proceeds in the enclosure. Unfortunately, due to lack of experimental data in the present configuration at these values of Ra, there is no experimental verification of sustained turbulence at large times, as the TL model predicts.

The studies of Evans et al. [5] and Hess and Miller [7] have approached the problem analytically by dividing the fluid region into a boundary layer region along the heated wall, a mixing region at the top and a stratified core and modelling each of these independently with suitable matching conditions. Although the results obtained here do exhibit such clearly defined regions, which corroborate the analysis followed in the above

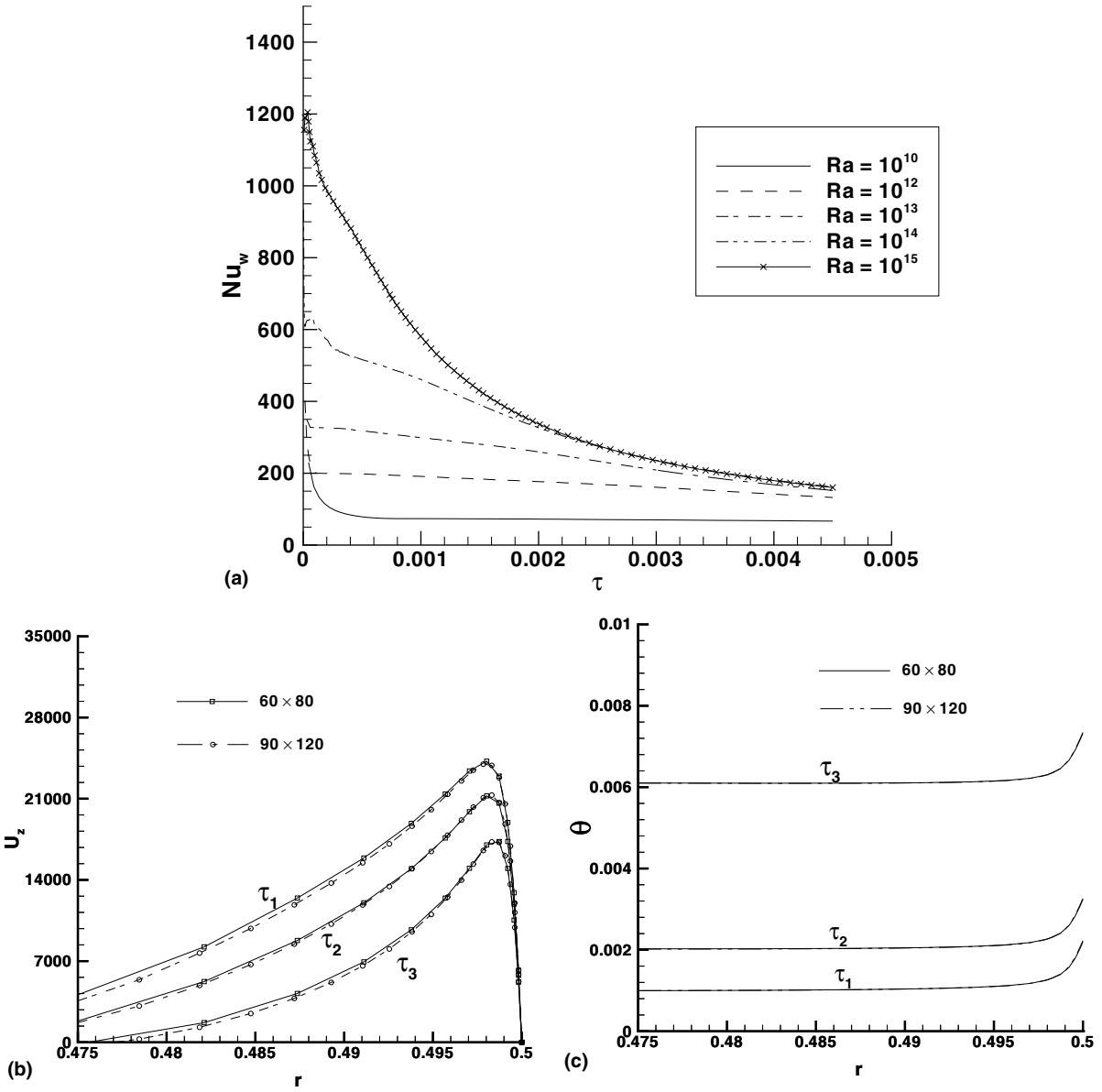

Fig. 10. (a) Mean wall Nusselt number vs. time for both laminar and turbulent flow solutions (b) axial velocity and (c) temperature profiles obtained with the TL model for $Ra = 10^{14}$, at $Z = 0.5$, $\tau_1 = 7.5 \times 10^{-4}$, $\tau_2 = 1.5 \times 10^{-3}$ and $\tau_3 = 4.5 \times 10^{-3}$ and effect of grid dimensions.

studies, it should be noted that in the transient state at the present high values of *Ra* there is a large number of secondary flows that develop in the enclosure, as shown in Figs. 5 and 7 especially near the axis and towards the bottom. These originate from the downward movement of the hot fluid from the top surface into the core along the axis and tend to build and vanish periodically, leading to an oscillatory behavior. These phenomena have a strong influence on the overall transient behavior of the system, affecting the development of the boundary layer along the heated wall and the stratification in the core. In other words, they enhance the elliptic nature of the whole system, a fact which is only accounted for in a full elliptic numerical simulation.

4.3.3. Vertical wall heat transfer and temperature distributions

In Fig. 10(a) the time variation of the mean wall Nusselt number over the heated wall is shown in the range $Ra = 10^{10}$–10^{15}, so that a comparison between

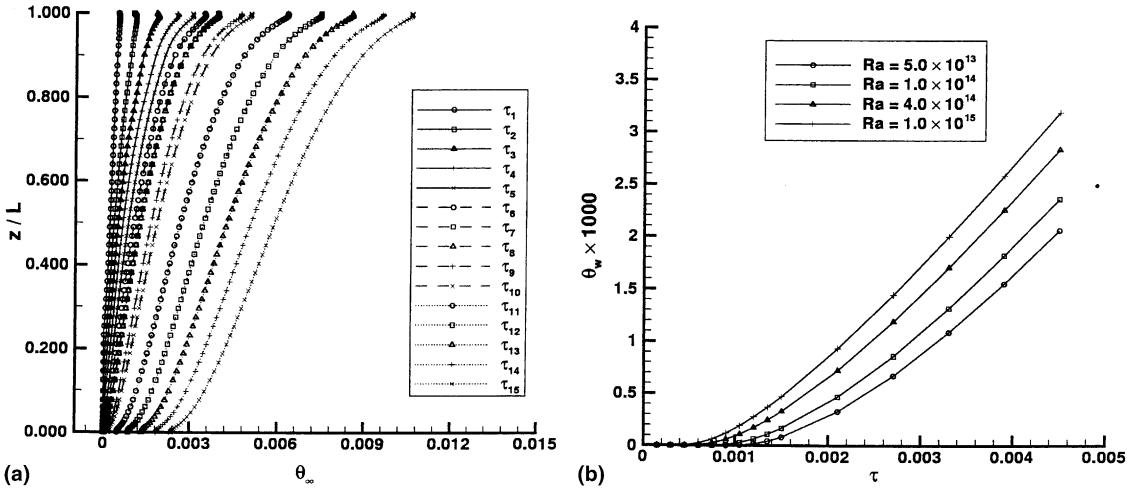

Fig. 11. Transient temperature results obtained with the AKN model. (a) Typical development of the vertical core temperature distribution with time at $Ra = 10^{14}$. $\tau_1 - \tau_{10}$: interval is 1.5×10^{-4} and 6×10^{-3} afterwards. (b) Bottom surface temperature at $r = 0.25$ vs. time.

Table 2
Heat-up time scales for $Ra = 5.0 \times 10^{13}$–10^{15}

Ra	$\tau_h \times 10^3$	t_h (s)
5×10^{13}	1.5763	138.2
10^{14}	1.27126	111.4
4×10^{14}	0.901142	79.0
10^{15}	0.696933	61.0

The physical times are for an enclosure with the conditions of [5] and with $L/D = 1$ (0.2032 m high).

simulations for laminar ($Ra = 10^{10}$–10^{13}) and turbulent ($Ra = 10^{14}$–10^{15}) flow can be directly realized. It can be observed that the curves for laminar flow reach a plateau within shorter times than those for turbulent flow. The decrease to an almost constant value attained at large times is shown to be monotonic, while in the turbulent flow results there is an initial rise in the values, followed by a decrease to the quasi-steady values. These final values may also be observed not to vary significantly with Ra for $Ra \geqslant 10^{13}$. Figs. 10(b and c) show the axial velocity and temperature profiles at mid-height, as computed by the TL model at three different time instants and for two different grids. These figures justify the choice of the 60×80 grid as the base grid for the transient, turbulent flow simulations, since the discrepancies between this grid and the next finer, 90×120, are almost non-existent for the temperature, and very small for the velocities and present only at early times. At later times than shown here, the discrepancies become even smaller. Both grids are shown to capture the profiles quite well and the grid effect is similar for the other turbulence models.

Fig. 11(a) shows the development of the temperature stratification in the core with time at $Ra = 10^{14}$ computed by the AKN model. The increase in the slope of the curves with time becomes obvious and the mixing zone at the top [5] can be shown to extend up to $z/L = 0.8$, while the bottom layer extends up to about $z/L = 0.1$. In between, the temperature distribution is almost linear and this section can be used to determine the core temperature gradient at each time instant. In Fig. 11(b) the bottom surface temperature with time at different Rayleigh numbers is shown at $r = 0.25$. This plot is indicative of the time at which the temperature front [35] reaches the bottom as stratification builds up and it can be seen to reduce with an increase in Ra. In order to estimate some typical heat-up time scales τ_h in this case of constant-heat-flux heating, it is necessary to define a charateristic temperature. Since there are no temperatures that remain constant with time here, we use the normalized temperature θ_w/θ_B, i.e., divided by the bulk fluid temperature defined earlier and take the time needed until the normalized bottom surface temperature at $r = 0.25$ reaches the value of 0.05. This is in accordance with the criterion used in [10,35]. The results are shown in Table 2, both in dimensionless and in physical times, for which water properties at 60 °C and an enclosure with $L = 0.2032$ m have been assumed [5].

In Fig. 12 the vertical temperature gradient at the core θ'_∞, computed by the various turbulence models for $Ra = 5 \times 10^{13}$–10^{15}, is plotted against a dimensionless time parameter, as defined by Evans et al. [5]. The solid line shown has been obtained by the following analytically derived correlation which was found to best fit the experimental turbulent flow data for water [5]:

$$\theta'_\infty = 11.5 \frac{Pr^{7/45} Fo^{8/15}}{Ra^{2/15}}. \quad (15)$$

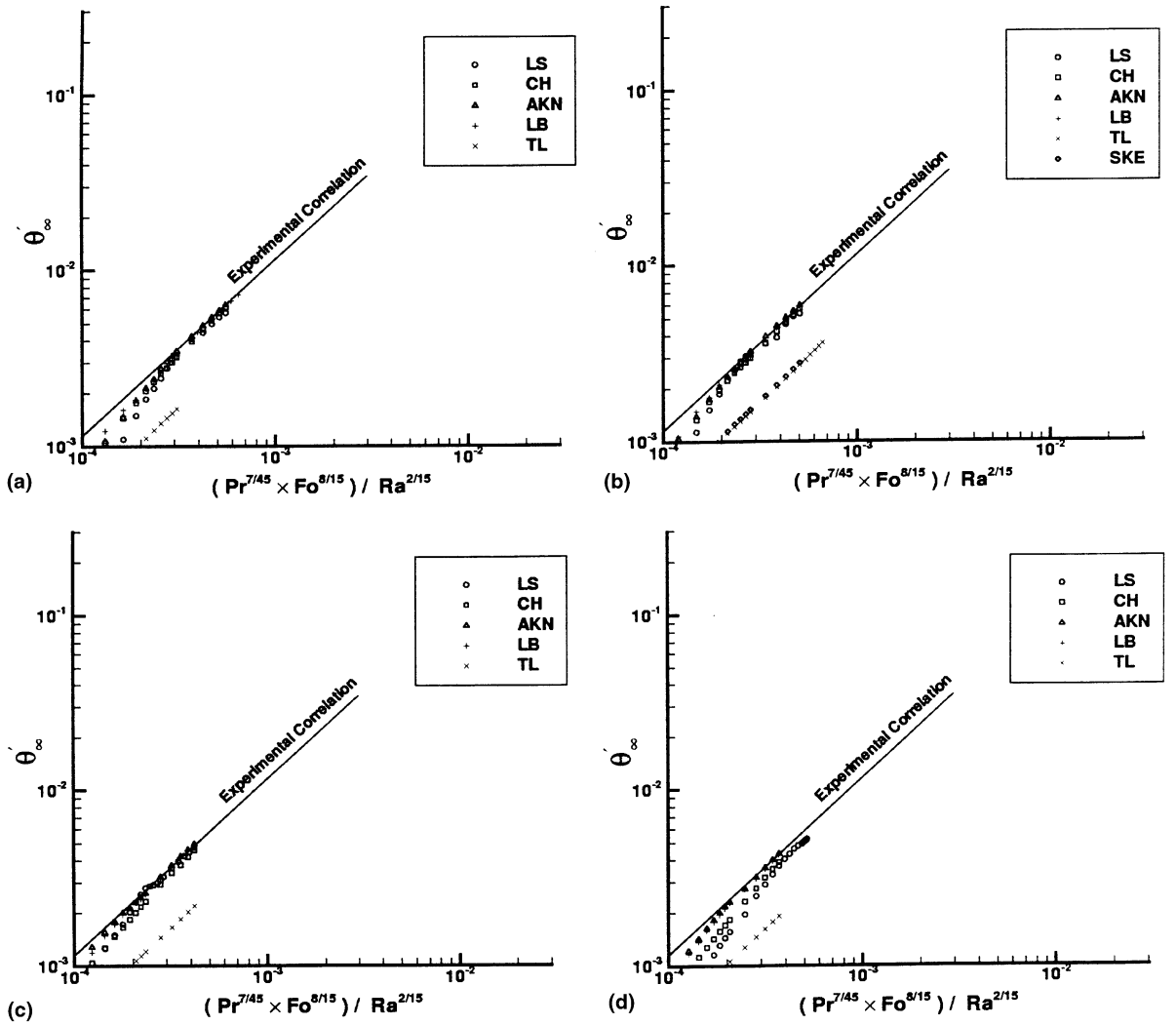

Fig. 12. Vertical core temperature gradient variation computed by various models vs. experimental correlation [5] for: (a) $Ra = 5 \times 10^{13}$, (b) $Ra = 10^{14}$, (c) $Ra = 4 \times 10^{14}$ and (d) $Ra = 10^{15}$.

The present results seem to approach the correlating line after the early transient period, at a rate which varies between the models, and generally show good agreement. The AKN model appears to approach the correlating line sooner than other models at most *Ra* values, followed closely by the LB model and then by the remaining low-*Re* models. The TL seems to yield θ'_{∞} values which follow a line parallel to that of Eq. (15). As already discussed, the TL model, unlike other models, does not predict relaminarization and this fact alone may be sufficient to justify the deviation. The present results suggest, therefore, that the data that correlate well to Eq. (15) correspond to core temperature distributions that have developed after boundary layer transition and relaminarization has taken place, although there is no discussion of such a phenomenon in [5]. Indeed, in Fig. 12(d) for $Ra = 10^{15}$, where relaminarization was found to occur at later times than for lower *Ra*, the results of the LS and CH models approach the correlating line at later times. For the TL model, a different coefficient than 11.5 in Eq. (15) was sought and was found that a value around 5.5 would correlate the data quite well. Comparing the data obtained by the SKE model for one value of *Ra* (Fig. 12(b)) showed a good agreement with the TL model data, indicating that it is the high-*Re* form common to these two models that leads to the differences in the behavior with the rest of the models.

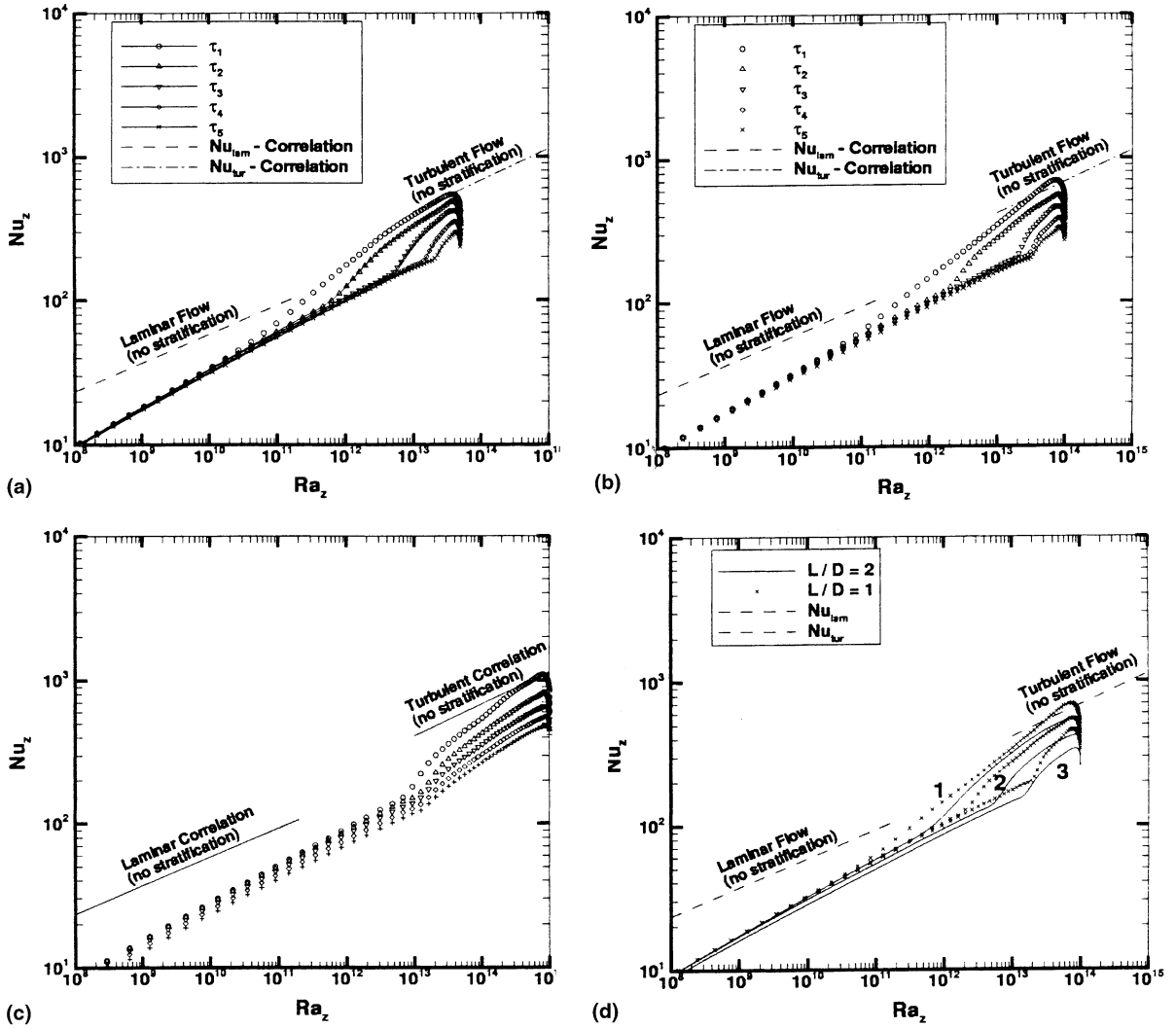

Fig. 13. Local wall Nusselt number vs. local Rayleigh number computed by the LS model at early times ($\tau \leqslant 7.5 \times 10^{-4}$) and for: (a) $Ra = 5 \times 10^{13}$, (b) $Ra = 10^{14}$ and (c) $Ra = 10^{15}$. In (d) the effect of increasing the aspect ratio to $L/D = 2$ is shown, at the first three time instants and for $Ra = 10^{14}$. The correlations shown are from measurements on a flat surface [33].

4.3.4. Boundary layer transition and relaminarization

Fig. 13 is a plot of the local Nusselt vs. the local Rayleigh number along the lateral surface at different time instants, revealing the development of the boundary layer along the wall. Here results are plotted for the LS model, however the other models behave similarly. The boundary layer transition at early times becomes evident, when comparing against the experimentally obtained correlation for turbulent flow along a flat surface by Vliet and Liu [33]. That correlation was derived in the absence of stratification, which resembles the present situation only at early times. Hence the good agreement with the correlation at the first two time instants in Fig. 13. As time proceeds, there is an increasing departure from the correlation, even though the transition is still discernible in the curve for some time. Interestingly enough, the laminar boundary layer does not compare well, as the values of the Nusselt number are significantly lower than the correlation for the laminar regime [33]. This fact may be attributed to the influence of stratification.

Due to space limitations, the effect of the aspect ratio could not be considered in the present study. However, some calculations were performed for an enclosure with $L/D = 2$ as well, at $Ra = 10^{14}$ and with the LS model and the effect of L/D on the Nusselt number can be realized in Fig. 13(d). By comparing the results for $L/D = 1$ and $L/D = 2$ it can be observed that the

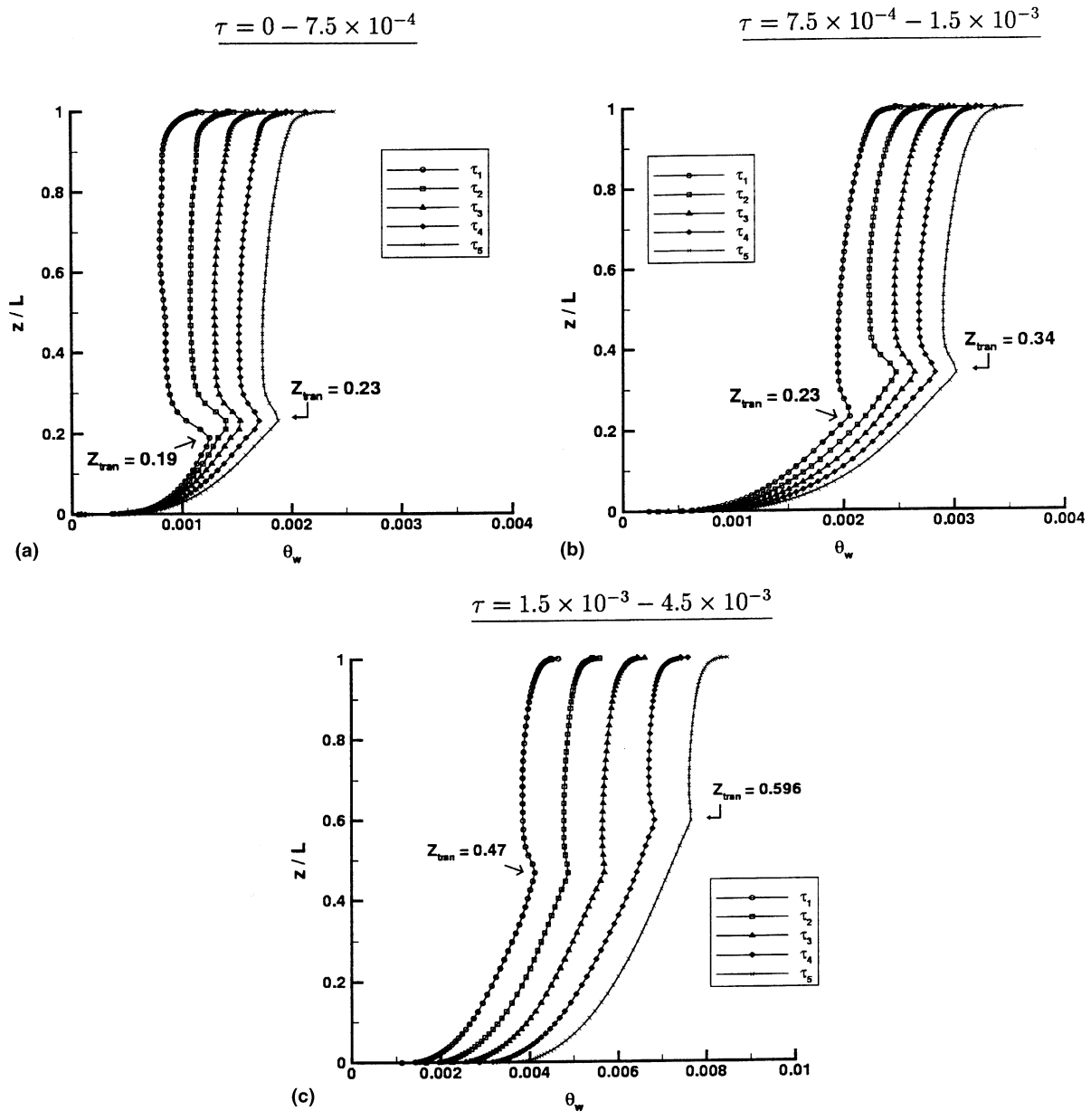

Fig. 14. Lateral wall temperature variation at different time instants and for $Ra = 10^{15}$ computed with the LS model. Interval between time instants in (a) and (b): 1.5×10^{-4} and in (c) 6×10^{-4}. The shifting of the transition point as time lapses is shown.

increased stratification at $L/D = 2$ leads to a delayed boundary layer transition and generally lower values of the Nusselt number compared to the base aspect ratio of $L/D = 1$. The laminar-to-turbulent transition may also be observed based on the criterion of the maximum of the wall temperature of Vliet and Liu [33]. This is shown in Fig. 14 at different time instants and for $Ra = 10^{15}$. A local maximum can be observed at all times, indicating the transition point, which gradually moves upward until the curves smoothen out as the flow heads toward laminarization.

5. Conclusions

The natural convection in a vertical cylindrical enclosure heated from the sidewall at constant heat flux was studied numerically at high Rayleigh numbers,

ranging from the laminar into the turbulent flow regime. The general qualitative features, previously analyzed in similar configurations, consisting of the development of a vertical thermal boundary layer interacting with a mixing zone at the top and a stratified core were verified, however these were here shown to be accompanied by a strong secondary-flow activity during transients, which largely affects the thermal mixing. In laminar flow, results exhibited a generally good agreement with relevant experimental data, even though in the early stages of the development of the transient thermal field good quantitative agreement was not obtained, even with fine grids. This could perhaps be improved by using a numerical scheme of higher-order in time. In turbulent flow, boundary layer transition was obtained along the heated wall, following which the low-*Re* turbulence models used predicted a laminarization under the action of thermal stratification. On the contrary, the two-layer model yielded a boundary layer which remained turbulent even at large times, with a maximum turbulent viscosity 20–25 times the laminar viscosity. The pattern of transition followed by relaminarization agreed well with previous analytically derived and experimentally confirmed correlations for the time evolution of the temperature gradient in the core. However, the experimental results available do not extend to Rayleigh numbers high enough to describe the turbulent flow regime so that the numerically predicted trends can be more extensively compared and verified.

References

[1] V. Belessiotis, D. Haralambopoulos, Testing solar water heating systems in Athens, Greece, Solar Energy 50 (2) (1993) 167–177.

[2] P. Mavros, V. Belessiotis, D. Haralambopoulos, Stratified energy storage vessels: characterization of performance and modeling of mixing behavior, Solar Energy 52 (4) (1994) 327–336.

[3] G. de Vahl Davis, Natural convection of air in a square cavity: a bench mark numerical solution, Int. J. Numer. Meth. Fluids 3 (1983) 227–248.

[4] R.A.W.M. Henkes, C.J. Hoogendoorn, Comparison exercise for computations of turbulence natural convection in enclosures, Numer. Heat Transfer, Part B 28 (1995) 59–78.

[5] L.B. Evans, R.C. Reid, E.M. Drake, Transient natural convection in a vertical cylinder, AIChE J. 14 (2) (1968) 251–259.

[6] C.F. Hess, C.W. Miller, Natural convection in a vertical cylinder subject to constant heat flux, Int. J. Heat Mass Transfer 22 (1979) 421–430.

[7] C.F. Hess, C.W. Miller, An experimental and numerical study on the effect of the wall in a thermocline-type cylindrical enclosure (I and II), Solar Energy 28 (2) (1982) 145–161.

[8] D.E. Daney, Turbulent natural convection of liquid deuterium, hydrogen and nitrogen within enclosed vessels, Int. J. Heat Mass Transfer 19 (1976) 431–441.

[9] R.J. Shyu, C.K. Hsieh, A numerical study of unsteady natural convection in a storage tank, in: B.H. Glenn (Ed.), Progress in Solar Energy (6), Proceedings of the 1984 Annual Meeting of the American Solar Energy Society, Anaheim, CA, 1984, pp. 307–314.

[10] J.M. Hyun, Transient process of thermally stratifying an initially homogeneous fluid in an enclosure, Int. J. Heat Mass Transfer 27 (10) (1984) 1936–1938.

[11] Y.S. Lin, R.G. Akins, Thermal description of pseudo-steady-state natural convection inside a vertical cylinder, Int. J. Heat Mass Transfer 29 (2) (1986) 301–307.

[12] Y.S. Lin, R.G. Akins, Pseudo-steady-state natural convection heat transfer inside a vertical cylinder, ASME J. Heat Transfer 108 (1986) 310–316.

[13] J. Sun, P.H. Oosthuizen, Transient natural convection in a vertical cylinder with a specified wall flux, in: R.K. Shah (Ed.), Proceedings of the 1989 National Heat Transfer Conference, HTD(107), ASME, Philadelphia, PA, 1989, pp. 305–314.

[14] A. Lemembre, J.-P. Petit, Laminar natural convection in a laterally heated and upper cooled vertical cylindrical enclosure, Int. J. Heat Mass Transfer 41 (16) (1995) 2437–2454.

[15] W. Lin, S.W. Armfield, Direct simulation of natural convection cooling in a vertical circular cylinder, Int. J. Heat Mass Transfer 42 (1999) 4117–4130.

[16] M. Holzbecher, A. Steif, Laminar and turbulent free convection in vertical cylinders with internal heat generation, Int. J. Heat Mass Transfer 38 (15) (1995) 2893–2903.

[17] E.M. Sparrow, F. Samie, Interaction between a stream which passes through an enclosure and natural convection within the enclosure, Int. J. Heat Mass Transfer 25 (10) (1982) 1489–1502.

[18] A. Bouhdjar, A. Benkhelifa, A. Harhad, Numerical study of transient mixed convection in a cylindrical cavity, Numer. Heat Transfer, Part A 31 (1997) 305–324.

[19] E. Hahne, Y. Chen, Numerical study of flow and heat transfer characteristics in hot water stores, Solar Energy 64 (1–3) (1998) 9–18.

[20] J.M. Hyun, Unsteady buoyant convection in an enclosure, Adv. Heat Transfer 24 (1994) 277–321.

[21] E.L. Papanicolaou, Y. Jaluria, Computation of turbulent flow in mixed convection in a cavity with a localized heat source, ASME J. Heat Transfer 117 (3) (1995) 649–658.

[22] W. Rodi, Experience with two-layer models combining the k–ϵ model with a one-equation model near the wall, Paper 91-0216, in: Proceedings of the 29th Aerospace Sciences Meeting, AIAA, Reno, NV, January 1991.

[23] B.E. Launder, D. Spalding, The numerical computation of turbulent flows, Comput. Meth. Appl. Mech. Eng. 3 (1974) 269–289.

[24] B.E. Launder, B.I. Sharma, Application of the energy-dissipation model of turbulence to the calculation of flow near a spinning disc, Lett. Heat Mass Transfer 1 (1974) 131–138.

[25] K.-Y. Chien, Predictions of channel and boundary-layer flows with a low-Reynolds-number turbulence model, AIAA J. 20 (1982) 33–38.

[26] K. Abe, T. Kondoh, Y. Nagano, A new turbulence model for predicting fluid flow and heat transfer in separating and reattaching flows – I. Flow field calculations, Int. J. Heat Mass Transfer 37 (1994) 139–151.

[27] C.K.G Lam, K.A. Bremhorst, Modified form of the k–ϵ model for predicting wall turbulence, ASME J. Fluids Eng. 103 (1981) 456–460.

[28] L. Davidson, Calculation of the turbulent buoyancy-driven flow in a rectangular cavity using an efficient solver and two different low Reynolds k–ϵ turbulence models, Numer. Heat Transfer, Part A 18 (1990) 129–147.

[29] W. Xu, Q. Chen, F.T.M. Nieuwstadt, A new turbulence model for near-wall natural convection, Int. J. Heat Mass Transfer 41 (1998) 3161–3176.

[30] J. Zhu, A low-diffusive and oscillation-free convection scheme, Commun. Appl. Numer. Meth. 7 (1991) 225–232.

[31] R. Cheesewright, K.J. King, S. Ziai, Experimental data for the validation of computer codes for the prediction of two-dimensional buoyant cavity flows, in: J.A.C. Humphrey, et al. (Eds.), Significant Questions in Buoyancy Affected Enclosure or Cavity Flows, HTD(60), ASME, Philadelphia, PA, 1986, pp. 75–81.

[32] E.M. Sparrow, J.L. Gregg, Laminar free convection from a vertical plate with uniform surface heat flux, Trans. ASME 78 (1956) 435–440.

[33] G.C. Vliet, C.K. Liu, An experimental study of turbulent natural convection boundary layers, ASME J. Heat Transfer 91 (1969) 517–531.

[34] Z.H. Qureshi, B. Gebhart, Transition and transport in buoyancy driven flow in water adjacent to a vertical uniform flux surface, Int. J. Heat Mass Transfer 21 (1978) 1467–1479.

[35] J.M. Hyun, Propagation of the temperature front in heat-up of an initially isothermal fluid, Int. J. Heat Mass Transfer 29 (3) (1984) 499–501.